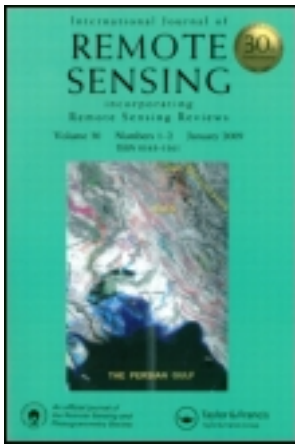


This article was downloaded by: [The Nasa Goddard Library]

On: 06 September 2012, At: 08:07

Publisher: Taylor & Francis

Informa Ltd Registered in England and Wales Registered Number: 1072954 Registered office: Mortimer House, 37-41 Mortimer Street, London W1T 3JH, UK



## International Journal of Remote Sensing

Publication details, including instructions for authors and subscription information:

<http://www.tandfonline.com/loi/tres20>

### A case for natural colour imagery from geostationary satellites, and an approximation for the GOES-R ABI

Steven D. Miller<sup>a</sup>, Christopher C. Schmidt<sup>b</sup>, Timothy J. Schmit<sup>c</sup> & Donald W. Hillger<sup>d</sup>

<sup>a</sup> Cooperative Institute for Research in the Atmosphere (CIRA), Colorado State University, Fort Collins, CO, USA

<sup>b</sup> Cooperative Institute for Meteorological Satellite Studies (CIMSS), Space Science and Engineering Center (SSEC), University of Wisconsin-Madison, Madison, WI, USA

<sup>c</sup> Advanced Satellite Products Branch (ASPB), NOAA/NESDIS-STAR, Madison, WI, USA

<sup>d</sup> Regional and Mesoscale Meteorology Branch (RAMMB), NOAA/NESDIS-STAR, Fort Collins, CO, USA

Version of record first published: 13 Dec 2011

To cite this article: Steven D. Miller, Christopher C. Schmidt, Timothy J. Schmit & Donald W. Hillger (2012): A case for natural colour imagery from geostationary satellites, and an approximation for the GOES-R ABI, *International Journal of Remote Sensing*, 33:13, 3999-4028

To link to this article: <http://dx.doi.org/10.1080/01431161.2011.637529>

PLEASE SCROLL DOWN FOR ARTICLE

Full terms and conditions of use: <http://www.tandfonline.com/page/terms-and-conditions>

This article may be used for research, teaching, and private study purposes. Any substantial or systematic reproduction, redistribution, reselling, loan, sub-licensing, systematic supply, or distribution in any form to anyone is expressly forbidden.

The publisher does not give any warranty express or implied or make any representation that the contents will be complete or accurate or up to date. The accuracy of any instructions, formulae, and drug doses should be independently verified with primary

sources. The publisher shall not be liable for any loss, actions, claims, proceedings, demand, or costs or damages whatsoever or howsoever caused arising directly or indirectly in connection with or arising out of the use of this material.

## A case for natural colour imagery from geostationary satellites, and an approximation for the GOES-R ABI

STEVEN D. MILLER\*†, CHRISTOPHER C. SCHMIDT‡, TIMOTHY J.  
SCHMIT§ and DONALD W. HILLGER¶

†Cooperative Institute for Research in the Atmosphere (CIARA), Colorado State University,  
Fort Collins, CO, USA

‡Cooperative Institute for Meteorological Satellite Studies (CIMSS), Space Science and  
Engineering Center (SSEC), University of Wisconsin-Madison, Madison, WI, USA

§Advanced Satellite Products Branch (ASPB), NOAA/NESDIS-STAR, Madison, WI, USA

¶Regional and Mesoscale Meteorology Branch (RAMMB), NOAA/NESDIS-STAR,  
Fort Collins, CO, USA

(Received 15 December 2010; in final form 28 October 2011)

‘Natural’ (or ‘true’) colour imagery, so-called for its qualitative likeness to colour photography, is one of the most visually intuitive and readily communicable forms of satellite information. It is constructed by combining solar reflectance measurements from three narrow spectral bands defining the red, green and blue wavelengths of visible light. Natural colour facilitates the interpretation of multiple components in the complex earth/atmosphere scene and, therefore, it is widely used by experts and non-experts alike to visualize many forms of geophysical phenomena. Although sensors on board low-Earth-orbiting (LEO) satellites have long-demonstrated the superior quality of natural colour imagery over various other ‘false colour’ renditions, similar capabilities currently do not exist on sensors operating in geostationary orbits that offer distinct advantages over LEO in terms of high temporal refresh. The Advanced Baseline Imager (ABI) of the next-generation Geostationary Operational Environmental Satellite (GOES)-R series will include the blue and red bands, but is missing the 0.55  $\mu\text{m}$  green band necessary for producing natural colour. The emphases of this article are twofold. First, we consider the merits of natural colour imagery from the standpoints of both science and operational users, and the philosophical roadblocks of a system definition process that seems inherently ill-equipped to consider qualitative user requirements. Second, we present a mitigation strategy for GOES-R ABI that entails synthesizing the missing ABI green band information via its correlation with spectrally adjacent available bands, with a first-order account for surface type dependencies. The technique is developed, demonstrated and evaluated here using Moderate-resolution Imaging Spectroradiometer (MODIS) data.

### 1. Introduction

Satellite environmental remote sensing has come a long way from the simple radiometer instruments that flew on early technology demonstration systems of the 1960s, when the principle mission objective was simply to gain a better vantage point on the meso/synoptic-scale structure of cloud cover. On 1 April 1960, the Television

---

\*Corresponding author. Email: miller@cira.colostate.edu

Infrared Observation Satellite (TIROS) provided the first 'television picture' from space (Wark and Popham 1960). These seminal views of the Earth and its weather from space came at the expense of coarse resolution, grainy pictures replete with noise and other sensor-related artefacts.

Since those pioneering efforts, advances in both the design and fabrication of radiometer technology have yielded far more sophisticated sensors in terms of spatial, temporal, spectral and radiometric resolution performance. With these advances came the ability to resolve and quantify the observable scene in new ways bearing higher relevance to environmental characterization and numerical weather prediction. As we look towards the future capabilities of sensors on environmental satellite programmes, baseline performance research and operational expectations have expanded significantly.

A fundamental role of satellite imaging radiometers is to facilitate environmental characterization by human analysts. The focal point of the current research is on daytime visible measurements of reflected sunlight and the ability of satellite imaging radiometers to depict objects in the scene in values of hue/saturation that are reminiscent to those of a colour photograph. This so-called natural colour or true colour technique is particularly useful to human analysts of satellite imagery, as it takes advantage of our inherent familiarity with colour interpretation and offers a very broad range of information content through colour that cannot be represented via limited colour space or greyscale renditions.

The operational need for higher time refresh can be met via a constellation of polar orbiting sensors that possess the required channels for producing natural colour. However, complications arising from different sensor characteristics (e.g. instrument response), spatial resolution, scanning pattern, anisotropic properties of the scene and parallax effects (issues arising from changing sensor geometry) and irregular time sampling can lead to a variety of undesirable effects when animating the series of images. A superior alternative is to leverage the geostationary (GEO) orbit to collect a series of geometrically consistent imagery. The GEO orbit (approximately 36 000 km above mean sea level and coincident with the Earth's equatorial plane) provides an orbital period matching the rotation rate of the Earth and thus appears to hover over a given point on the surface. At only one time in the history of satellite remote sensing has a sensor in GEO orbit been capable of providing a version of natural colour from its native channel suite. Launched in 1967, the NASA Applications Technology Satellites-3 (ATS-3) geostationary sensor (parked initially at 45° W and drifting to 95° W by the end of 1978) provided the first natural colour imagery at half-hourly intervals via a multispectral spin-scan cloud camera (Suomi and Parent 1968, Warnecke and Sunderlin 1968). The red and blue channels failed after only 3 months, and as of 1974 the camera was no longer providing useful data. Over four decades since the launch of ATS-3, it remains the only satellite to provide a direct, albeit fleeting, capability to render natural colour imagery from geostationary orbit.

In 2015, the National Oceanic and Atmospheric Administration (NOAA) will launch the first in a series of next-generation Geostationary Operational Environmental Satellites (GOES), which began with GOES-1 in 1975. Assigned alphabetical values until placed into the proper geostationary orbit (whereupon they receive a numeric identifier), the first instalment of this new satellite series is referred to as GOES-R (Gurka and Dittberner 2001) and will be commissioned as GOES-16. GOES-R represents a paradigm shift to the GOES programme in terms of

remote-sensing capabilities. Included among its sensor suite is the first lightning mapper to fly in GEO orbit (the GOES Lightning mapper, GLM; Goodman *et al.* 2006), an improved imaging radiometer called the Advanced Baseline Imager (ABI) and several space weather sensors. Details of the ABI and its 16 narrow-band channels spanning the optical spectrum ( $\sim 0.4\text{--}13.6\ \mu\text{m}$ ), along with a discussion of new/improved environmental data record (EDR) is presented by Schmit *et al.* (2005) and summarized in table 1.

The objectives of this article are twofold. First, we address the use of natural colour imagery from geostationary satellites, beginning with an overview of the practical uses for imagery. We hold this discussion in the context of the GOES-R ABI, which, despite its many advances over the heritage GOES, imagers will not provide

Table 1. Summary of the wavelengths, resolution and sample use of the ABI bands (adapted from Schmit *et al.* (2005)).

ABI band number	Wavelength range ( $\mu\text{m}$ )	Nominal central wavelength ( $\mu\text{m}$ )	Nominal sub-satellite IGFOV (km)	Sample application
1	0.45–0.49	0.47	1	Daytime aerosol-over-land, coastal water mapping
2	0.59–0.69	0.64	0.5	Daytime clouds, fog, insolation, winds
3	0.84–0.88	0.86	1	Daytime vegetation/burn scar and aerosol-over-water, winds
4	1.365–1.395	1.38	2	Daytime cirrus cloud
5	1.58–1.64	1.61	1	Daytime cloud-top phase and particle size, snow
6	2.235–2.285	2.26	2	Daytime land/cloud properties, particle size, vegetation, snow
7	3.80–4.00	3.90	2	Surface and cloud, fog at night, fire, winds
8	5.77–6.60	6.19	2	High-level atmospheric water vapour, winds, rainfall
9	6.75–7.15	6.95	2	Mid-level atmospheric water vapour, winds, rainfall
10	7.24–7.44	7.34	2	Lower-level water vapour, winds and SO <sub>2</sub> (volcanic)
11	8.3–8.7	8.5	2	Total water for stability, cloud phase, dust, SO <sub>2</sub> , rainfall
12	9.42–9.80	9.61	2	Total ozone, turbulence and winds
13	10.1–10.6	10.35	2	Surface and cloud properties
14	10.8–11.6	11.2	2	Imagery, sea surface temperature (SST), clouds, rainfall
15	11.8–12.8	12.3	2	Total water, ash and SST
16	13.0–13.6	13.3	2	Air temperature, cloud heights and amounts

Notes: The minimum and maximum wavelength range represent the full-width at half-maximum (FWHM or 50%) points. IGFOV is the instantaneous geometric field of view.

a capability for natural colour imagery from its native channel suite. Overcoming this problem forms the second objective of this article. Here, we present a correlative technique to synthesize the green band necessary to approximate natural colour from the ABI, and demonstrate through examples from the Moderate-resolution Imaging Spectroradiometer (MODIS) the performance expectations and limitations. The technique is proposed as a means to render natural colour imagery from the GOES-R ABI.

Our analysis indicates that the missing green band can be simulated via the proposed technique to within 0.5% (reflectance units (0,100)) over most scenes. The greatest challenge for the technique, which relies heavily on a strong correlation between the green band and the reflective infrared band ( $\sim 0.865 \mu\text{m}$ ) related to chlorophyll, occurs for shallow water regions (e.g. shoals, where green tonality arises for reasons other than chlorophyll) and areas of high ocean colour (e.g. phytoplankton blooms). Here, local relative errors can exceed 25% and are visually discernible in the imagery products, but can be mitigated in part (for shallow water zones) through the use of surface-type dependent look-up tables (LUTs).

## 2. Two perspectives on the usage of satellite imager data

Although the uses of environmental satellite digital data sets are far too many to list comprehensively, for the purposes of this discussion, we shall categorize them as belonging to one of two main application genres: those addressing ‘indirect’ and ‘direct’ environmental characterization. The differences between the two applications are important and have ramifications for the specification of sensor performance requirements during the formative (design) phase of an environmental observing system programme. In order to place into proper context the utility of satellite imagery as a core requirement of a broad community of users and to understand in particular natural colour imagery as an application whose importance stands on an equal footing to quantitative satellite EDRs, we briefly describe both categories of imager data usage.

Indirect usage of satellite imager data describes the incorporation (or ‘assimilation’) of these data (usually in the form of calibrated radiances or brightness temperatures, but sometimes EDRs themselves) into numerical models in order to help better characterize the model’s environmental state (e.g. temperature, moisture and wind profiles) at the time or temporal neighbourhood of the observations and thereby improve predictions of future states. Here, the data are not visualized directly, but instead are incorporated numerically to define the model’s virtual environment, which can then be visualized at past, current or future times. The extent to which the introduction of satellite data results in changes (or ‘innovations’) to the model’s environmental state at initial time (the ‘analysis’), or to trends in that state over a specified period of time (the ‘assimilation window’), depends on the relative uncertainties of several components. These include uncertainties in the measurements themselves, the model’s assumptions on the initial state (the ‘background’) and the method of translation from satellite measurements to the corresponding environmental state (via ‘inverse operators’). The process of incorporating observations within a weather/climate forecast model across space and time is thus a very practical and essential use of satellite data.

Direct use of satellite imager data, on the other hand, describes a genre of applications seeking to characterize and/or visualize various properties of the environment directly from the observations, presenting this information in the form of either

quantitative data sets (e.g. cloud cover masks, aerosol/cloud optical and geometric properties, temperature/moisture profiles, precipitation rate, sea surface temperature, etc.) or qualitative imagery that highlights some subset of the many elements coexisting within the observed scene (e.g. high-spatial-resolution views of cloud systems, snow cover, aerosol/dust/ash plumes, etc.). Although these characterizations sometimes leverage ancillary data from a forecast model (e.g. to constrain degrees of freedom in a physical retrieval, or provide background information in order to facilitate the enhancement of a feature of interest in imagery), the end result is identification and spatial/temporal characterization of a particular environmental attribute present in the observed scene. This attribute may hold value for the prediction of future environmental states and validating model predictions.

Typically, direct applications seek to preserve the highest possible spatial resolution available from the observing system (in contrast to indirect applications that apply the data to model resolutions), but in some cases may involve the aggregation of data to achieve sensitivity or assist in spatial analysis. In the case of value-added satellite *imagery*, it may also preserve other features that are not related directly to the attribute of interest but provide physical context to it (e.g. mountainous topography explaining the observed spatial distribution of valley fog or snow cover patterns or a thunderstorm complex explaining the presence of an observed dust front). The end user of satellite imagery applications is most often the human analyst, who incorporates the information (in some cases, along with model-based guidance) to address near-term operational needs. These users may include knowledge based on many years of imagery analysis, coupled with their background expertise in a specific discipline or regional familiarity, to leverage satellite imagery in ways that objective algorithms may not be able to replicate reliably even if all the contextual elements and associated physical processes were considered.

The point of this discussion is to realize the indirect *and* direct utility of satellite imagery and to perceive the operational relevance of each genre to various user communities. In many cases, the production of value-added imagery falls out as a by-product of sensors designed primarily with quantitative EDR specifications in mind. This is not always the case, however, and a philosophical conundrum emerges when the two needs are pitted against one another on a system with limited resources related to budget and/or engineering design requirements. GOES-R presents an interesting case study in this regard and one that we will explore further in the context of natural colour imagery and deletion of the green band from the GOES-R ABI channel suite.

### 3. Natural colour imagery

Natural colour imagery falls under the category of ‘direct’ satellite applications outlined earlier. It is designed to simulate human photopic (colour) vision by combining spectral band information in a way similar to the behaviour of the red-, green- or blue-band sensitive cone cells of the retina. For a satellite imaging radiometer, appropriate scaling of narrow-band red, green and blue band measurements results in imagery that resembles a colour photograph taken from space. Corrections to remove contributions from the scattering molecular atmosphere (Rayleigh scatter) in these bands provide further visual clarity to the details of the imagery, particularly to the features residing in the lower atmosphere and surface, and at higher sensor scan angles in which optical paths through the molecular atmosphere are greater.

Available from contemporary low-earth-orbiting (LEO) satellites as a by-product of sensors designed principally for quantitative applications (e.g. ocean colour), natural colour imagery has struggled to find by its own merit a niche within the design requirements of quantitative EDR-driven remote-sensing missions. The superior interpretive clarity of natural colour to standard single-band visible imagery accounts for its widespread usage by experts and non-experts alike when it is available. To imagery analysts, the wealth of additional information provided by natural colour as compared to the standard 8-bit greyscaled imagery (where only a small fraction of these 256 shades are in fact optically differentiable by the human eye) or false colour composites (which often require training to interpret) bolsters interpretive ability.

These arguments are best illustrated by an example. Shown in figure 1 are two versions of imagery from the MODIS (King *et al.* 1992) centred on the Bay of Biscay (45.0° N, 4.0° W), collected on 16 May 2004 at 1320 UTC (early afternoon, local time). Each image is approximately 250 m pixel resolution and 625 km on a side. Natural colour imagery, created from Rayleigh-corrected versions of the blue, green and red channels of MODIS (bands 3, 4 and 1, respectively), is shown in figure 1(a), and a greyscale version of this image (representing conventional greyscale visible imagery) is shown in figure 1(b). The complex feature spanning much of the Bay of Biscay is a massive phytoplankton bloom (at 'a'), composed of trillions of microorganisms in the surface waters. The natural colour image reveals that portions of the bloom are in fact composed of a species of phytoplankton called coccolithophores, which form calcite shells. The increased reflectivity of the calcite results in the brighter turquoise colourations. Closer to the shore of France, non-coccolithophore species produce a darker, emerald green tonality (at 'b'). The brightening waters to the west of the coccolithophore bloom are the result of sunlight reflection (sun-glint, at 'c') off the water surface. The greyscale image, while capturing the bright portions of the plume, fails to distinguish colouration changes that could relate to age and misses the darker green regions of phytoplankton altogether. Inland, over portions of northern Spain and western France, the natural colour imagery readily distinguishes between different ecosystem zones based on vegetation and soil types that are relegated to a limited range of grey shades in the conventional visible imagery. Natural colour also highlights the greenish-tan alluvial plumes of the Midouze (at 'd') and Garonne (at 'e') rivers as they drain into the bay, while a small patch of clouds along the French coast (at 'f') could easily be misconstrued as another alluvial plume in the greyscale image. Although not present in figure 1, colouration also provides analysts with a means to distinguish between clouds and various atmospheric aerosol constituents such as haze/pollution, biomass burning smoke, oil fire smoke and various mineral dust plumes.

Natural colour images such as the MODIS example can be rendered at various levels of fidelity from a number of different satellites. These capabilities have existed on selected sensors operating on LEO (and most commonly, sun-synchronous polar-orbits) platforms since the 1990s. Examples (to name several) of sensors capable of producing natural colour imagery from an international constellation of satellites include: (1) ocean-colour research-grade sensors such as the Sea-viewing Wide Field-of-view Scanner (SeaWiFS, on GeoEye's Orbview-2) and the Ocean Colour Monitor (OCM, on the Indian Space Research Organisation's (ISRO) Oceansat); (2) general surface/atmosphere research-grade sensors such as MODIS (on the National Aeronautics and Space Administration's (NASA's) Terra and Aqua satellites) and the Medium-resolution Imaging Spectrometer (MERIS, on the European

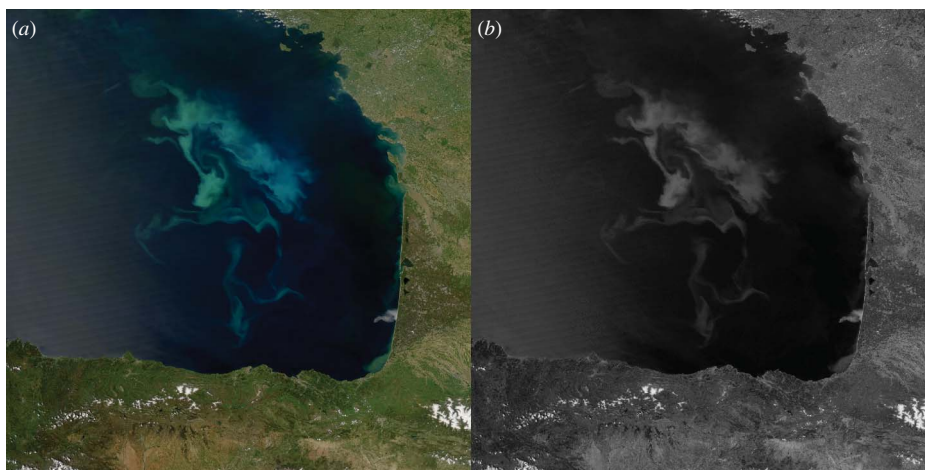


Figure 1. Natural colour (a) versus standard greyscale visible imagery (b) illustrates the superior capability of the former to highlight details of a phytoplankton bloom in the Bay of Biscay as observed by Terra MODIS on 16 May 2004 at 1320 UTC. Each panel is centred on 45.0° N, 4.0° W and is 625 km on a side. See text for labelled details.

Space Agency's (ESA's) Envisat; Curran and Steele 2005); and (3) very high spatial resolution (order of metres) commercial-grade sensors for surface mapping such as Ikonos and GeoEye-1 (both managed by GeoEye), the Landsat Thematic Mapper (managed by the United States Geological Survey (USGS)) and Satellite Pour l'Observation de la Terre (SPOT; managed by the Centre National d'Etudes Spatiales (CNES)). The major national operational satellite constellations of the USA (the Polar-orbiting Operational Environmental System (POES) operated by National Oceanic and Atmospheric Administration (NOAA)) and Europe (the MetOp satellite series operated by the European Organisation for the Exploitation of Meteorological Satellites (EUMETSAT)) currently do not provide radiometers capable of true colour imagery, but the USA will include the capability on its future operational LEO programme, the Joint Polar Satellite System (JPSS).

These LEO sensors generally offer high spatial and spectral resolution at the expense of coarse (1–2 daytime views per 24-hour period at equatorial and mid-latitudes) temporal resolution. The ability to loop such imagery is limited, and complicated by the various sensor characteristics and viewing geometries among various satellites contributing to the sequence. The following section details some of the merits of a GEO-based green band, which extend far beyond the band's utility in the context of natural colour imagery.

#### 4. A spectrum of practical reasons for a green band

There are many other justifications beyond natural colour for the inclusion of a geostationary-based radiometer featuring a green band. One important application of the green band is ocean colour remote sensing. Here, 0.55  $\mu\text{m}$  is the standard wavelength used for assessing chlorophyll-*a* concentration in phytoplankton. Yentsch (1960) describes how the progression of backscattered sunlight migrates from deep blue to green as pigmentation increases in phytoplankton. The preferential scattering

of green light by these pigments is exploited for ocean colour retrievals (e.g. Babin *et al.* 2003). O'Reilly *et al.* (1998) provide a thorough review on ocean colour chlorophyll algorithms, demonstrating the fundamental importance of the green band (in terms of the blue/green ratio) to these applications. Researchers monitor the spatiotemporal distribution of phytoplankton to climate change and the role of ocean biota in regulating the global carbon cycle (e.g. Frouin and Iacobellis 2002, Behrenfeld *et al.* 2005). In addition, harmful algal blooms (HABs) in coastal zones can introduce water toxicity levels that are lethal to aquatic plants and animals and are linked to human illness (e.g. Van Dolah 2000). Satellite-based detection and characterization of HABs (e.g. Kahru *et al.* 2004, Ahn *et al.* 2006) can be done from intermittent polar orbiter observations, but limited imagery refresh and the potential for cloud obscuration makes tracking these rapidly evolving events difficult. Here, a rapidly updating view of ocean colour features from geostationary orbit could be very helpful from a simple monitoring perspective.

Detection and characterization of atmospheric aerosol properties, and in particular the measurement of aerosol optical depth, is another important example where the 0.55  $\mu\text{m}$  band serves as a standard reference wavelength (e.g. Gonzales *et al.* 2000, Chowdhary *et al.* 2005, Ho *et al.* 2006). The need to characterize aerosol optical depth in this band also relates back to ocean colour applications. Since satellites observe the surface through the intervening atmosphere, which itself scatters green light by both molecular and aerosol particulates, measurements of the water leaving radiance (Gordon and Clark 1981) are typically an order of magnitude less than the top-of-atmosphere signal. This necessitates an atmospheric 'correction', which amounts to the simultaneous retrieval of aerosol and ocean colour properties in the green band (e.g. Stamnes *et al.* 2003). The increased temporal updates available from a geostationary-based sensor could improve these techniques, especially in regions of broken cloud.

There are important physical attributes to the green band that make it particularly valuable from the perspective of satellite imagery and interpretation by human analysts. This relevance is related to the optical response of the human eye to visible radiation. The eye is an organ that functions as a visible-spectrum (400–700 nm) radiometer with two 'modes' – photopic (daytime) and scotopic (night-time) vision. Light is focused onto the retina (at the rear of the eye), where it impacts on an array of photoreceptor cells known as cones and rods and is converted to an electric signal routed to the brain via the optic nerve. The cone cells are responsible for photopic vision and colour perception. Three types of cone cells, having peak absorptions at roughly 420–440, 534–545 and 564–580 nm, provide for colour sensitivity via differential stimulation of these cells (Wyszecki and Stiles 1982). Fu *et al.* (2010) provide an insightful discussion of how this process simplifies a spectrally complex scene to a set of discriminants that we refer to as colours and how this in turn relates to the concept of artificial colour imagery.

The eye is most sensitive to green band light because these frequencies reside near the peak sensitivity of two of the three cone cell types. The presence of green band information in satellite imagery thus provides specific detail to which the human eye is naturally attuned. When incorporated into a natural colour enhancement to simulate human vision, this detail is presented to the analyst in a way that minimizes interpretive training and expands the utility of satellite imagery to non-expert operational users and the general public.

Human interpretation of satellite data is of fundamental importance for many purposes (Sabins 1987). There is a diverse operational user base that stands to benefit from a geostationary natural colour capability. For example, some NOAA National Weather Service (NWS) forecasters use real-time satellite imagery for rapid assessment of regions under broken cloud cover. Here, the colours of land and ocean surfaces are readily distinguishable in contrast to greyscale imagery, which, depending on the surface reflectance properties, could be misconstrued for cloud. Other NWS forecasters monitor ice break-up over Lake Erie to assist in the deployment of an ice boom for the Niagara River. Here, natural colour provides improved contrast between ice and heavy/bright sediments in the lake, and such imagery from MODIS is currently used for this purpose despite its poor temporal refresh and susceptibility to cloud obscuration.

Natural colour images, even in their limited availability from a small collection of available LEO satellites, were in high demand by the US Department of Defense (DoD) during recent conflicts in the Middle East. Miller *et al.* (2006b) describe the use of LEO satellite imagery during Operation Iraqi Freedom (OIF), where high resolution natural colour imagery were in such high demand that the Commander, Naval Meteorology and Oceanography Command (CNMOC) funded the installation of X-band receiving stations at Navy Regional Centres in both Bahrain and Rota, Spain, to support operational demands for real-time imagery. Natural colour products were used during OIF by Navy and Air Force weather officers to monitor weather across southwest Asia, particularly in the context of overview graphics briefed to non-experts and discrimination of sand storms over land and water backgrounds.

## 5. Existing methods for natural colour approximation

User requests for natural colour satellite imagery have prompted various attempts to reproduce it from sensors that lack the full complement of red, green and blue bands. These approaches range widely in both algorithmic complexity and realism of the end results. Invariably, all approximations contain elements that differ from natural colour. Depending on the specific application and experience in satellite imagery interpretation, these differences may require little training or represent significant roadblocks. Described briefly here are several methods used for rendering approximate natural colour imagery from both polar and geostationary satellite systems.

Perhaps the most straightforward and universally applicable (in terms of the basic satellite band requirements) methods for approximating natural colour imagery involve simply the overlay of either visible or infrared data upon a natural colour background derived from an independent data source. Most imaging radiometers in orbit today, including the geostationary satellites, possess visible ( $\sim 0.65 \mu\text{m}$ ) and infrared-window ( $\sim 11 \mu\text{m}$ ) bands. Thresholds imposed on these data (e.g. reflectance exceeding a minimum value or brightness temperature below a maximum value) provide simple cloud-cover masks, based on the tendency for clouds to appear as brighter (visible) or cooler (infrared) than the clear-sky background in these bands. Limitations to this method include poor cloud detection (including false-cloud reported over highly reflective or cold surfaces), loss of cloud opacity information (no transparency against the colour background), misrepresentation of low-level or optically thin clouds as dark features and the reduced ability to distinguish among clouds, smoke and dust. In addition, the background coloured regions (clear sky) remain fixed over time.

Assigning a dynamically varying value transparency to the visible/infrared cloud data and allowing the colour background to 'transmit through' the non-opaque clouds improve the realism of the overlay-approach described earlier. A version of this technique, applied to various geostationary sensors and using the MODIS Blue Marble data set as its daytime background (and using at night a city lights mask derived from the DMSP Operational Linescan System), can be found on the *NexSat* website ([www.nrlmry.navy.mil/NEXSAT.html](http://www.nrlmry.navy.mil/NEXSAT.html); Miller *et al.* 2006a). Turk *et al.* (2010) invoke a similar dynamic transparency approach (embedding the information in the Alpha layer of a Portable Network Graphics image) to provide a semi-realistic view of the planet's weather for use in the near real-time global cloud weather layer of Google's 'Earth' virtual globe application. As with the non-dynamic overlay technique, the colour backgrounds typically are not current and will therefore miss evolving surface details such as natural disaster signatures (e.g. floods, mudslides, wild fires in progress and associated burn scar evolution) and other features (e.g. water turbidity, snow cover and seasonal vegetation changes).

Some satellite sensors provide bands in the near-infrared (NIR), where chlorophyll in vegetation is highly reflective. This information can be used as a first-order proxy for green vegetation, and can be enhanced accordingly (usually via a simple red/green/blue channel composite that inserts some function of daytime NIR data in the green band) to produce a pseudo-natural colour image. In this vein, EUMETSAT produces a 'natural colour' product from MSG Spinning Enhanced Visible and Infrared Imager (SEVIRI) data using the sensor's 0.6, 0.8 and 1.6  $\mu\text{m}$  spectral bands (e.g. [oiswww.eumetsat.org/IPPS/html/MSG/RGB/NATURALCOLOR/](http://oiswww.eumetsat.org/IPPS/html/MSG/RGB/NATURALCOLOR/)). The method succeeds in presenting vegetation in a green colour, and by construct is immune to the transparency artefacts of the overlay applications. Although the green appearance is 'false' with respect to natural colour, optically thick ice clouds appear cyan, low clouds appear slightly yellow, and there are potential ambiguities between optically thin cirrus and dust plumes that frequent the MSG field of regard, the EUMETSAT product is perhaps the closest self-contained geostationary approximation to natural colour available today.

The most sophisticated approaches to approximating natural colour involve quantitative manipulation of available channels in an effort to simulate missing channels, exploiting correlations between the available and missing information. Various examples of channel synthesis and cross-sensor relationships exist in the recent literature. Wang *et al.* (2006) provide a surrogate 1.6  $\mu\text{m}$  band for the faulty one on Aqua MODIS via polynomial regression using the nearby 2.1  $\mu\text{m}$  band for the purpose of improving snow detection capabilities. Falcone *et al.* (2007) use a canonical coordinate decomposition method to relate Meteosat-8 imagery data to MODIS-derived cloud products. More to the application of interest here, Chen and Tsai (1998) use an unsupervised fuzzy C-means classifier to represent the scene constituents, select spectral control points randomly from these classes, and apply a linear function to transfer SPOT imagery (which contains NIR, red and green bands but lacks the blue band) to Landsat Thematic Mapper (TM) natural imagery. The transformation coefficients are solved with the least-squares method for each C-means class, with fuzzy class membership allowing for contributions from multiple classes at varying weights. Using a similar approach to Chen and Tsai (1998), Patra *et al.* (2006) apply a linear scaling of the NIR, red and green bands of IKONOS to estimate the blue band. Their 'natural colour generator' technique uses a finite set of user-defined (i.e. manually selected) spectral control points, determining the relationship between the channels at those

points, and then applying the transformation to the false colour triplet in order to synthesize the blue band. Their transformation coefficients are adjustable, according to the radiometric resolution (i.e. bits-per-pixel) of the data being considered. The literature review conducted for the current research found no examples where transformations were applied to enable natural colour from geostationary observations or synthesize the green band.

## 6. Synthesizing green: a LUT approach

Approximation of natural colour imagery from GOES-R ABI must appeal to numerical approximations for constructing the green band. Described here is a statistical-based approach to approximating natural colour imagery, that is, in fact generally applicable to a radiometer providing two of the required three (red/green/blue) spectral bands. The basic approach, illustrated in figure 2, is similar to spectral transformation techniques of Chen and Tsai (1998) and Patra *et al.* (2006) in the sense that one sensor (here, MODIS) containing the red/green/blue/NIR is used to develop a relationship between one of the bands required for natural colour (here, the missing green band) and the available blue, red and NIR bands, with an eye towards applying this relationship to an independent sensor (here, GOES-R ABI). Unlike the previous methods, the current approach makes use of LUTs for the green band as a function of the B/R/NIR bands, generated from a composite of multiple observed scenes. It invokes a standardized version of ‘spectral control points’, in the form of surface-type-dependent tables, to better handle features holding weaker correlation between green and the available bands. Applied to the future GOES-R ABI, the anticipated result would appear similar to daytime GeoColor imagery (described previously) but with all parts of the image based on the currently observed data.

The complex spectral behaviour of earth scenes precludes a simple analytical relationship between values of the green band reflectance and those of the NIR, red and blue bands. Some scenes may not offer a collection of well-separated classifications to serve as the bases for linear relationships, and when they do, the relationships may be non-linear. To avoid making assumptions in this diverse spectral space, the current technique enlists LUTs to capture the dynamic range of observations for a

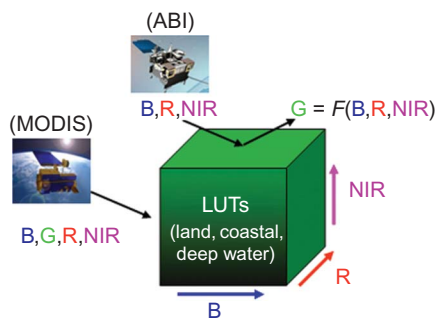


Figure 2. Simplified conceptual approach to synthesizing the green band (G) via look-up tables that represent green (G) as a function (F) of the blue (B), red (R) and near-infrared (NIR) band reflectance. All bands are corrected for molecular atmosphere scatter prior to populating/consulting the look-up tables (LUTs).

broad assortment of scenes collected globally. When applied to independent observations, the LUTs are consulted to provide an estimate of the green band reflectance for a given (red, blue, NIR) triplet for every pixel in the scene. An expanding search method (described later) is applied for rare cases where the LUT does not possess a valid value for the current triplet. After synthesizing the green band in this way, it is combined with the existing red and blue bands to form the natural colour imagery. Details of this process are provided next. Software for the new algorithm was written in the Interactive Data Language (IDL) and for demonstration purposes was built upon core processing routines for MODIS natural colour imagery written by Liam Gumley (Space, Science and Engineering Center (SSEC), University of Wisconsin-Madison), Jeffrey Schmaltz (NASA Goddard Space Flight Center (GSFC)) and Jacques Descloitres (while at NASA/GSFC).

The detailed procedure for constructing the LUTs, developed based on MODIS data, is as follows. First, to minimize the effects of sun/sensor geometry, all bands considered (B: 0.46–0.48  $\mu\text{m}$ , G: 0.55–0.57  $\mu\text{m}$ , R: 0.62–0.67  $\mu\text{m}$  and NIR: 0.84–0.88  $\mu\text{m}$ ) were corrected for atmospheric attenuation prior to populating the LUTs. Molecular, or Rayleigh scatter (e.g. Paltridge and Platt 1976), is highly dependent on wavelength (proportional to  $\lambda^{-4}$ ) and the sensor zenith angle, which combine to form a spectral optical path through the atmosphere, that is, biased strongly towards the shorter wavelength bands (B and G). For the current work, we enlisted atmospheric correction software developed by NASA's MODIS Rapid Response Project (<http://rapidfire.sci.gsfc.nasa.gov>). The software converts MODIS top-of-atmosphere calibrated radiances to atmospherically corrected (i.e. the atmospheric component of the signal removed) reflectance, accounting in a simple way for attenuation (absorption and scattering) and gain (scattering source) along the molecular path as defined by the sun–sensor geometry. These corrections were applied to the co-located MODIS 1 km resolution band data (it is essential for the LUT that all bands view the same earth locations).

To avoid any data modification arising from re-projection to a specific earth grid, the LUTs were built using the native sensor projection of MODIS. Two versions of LUTs were produced: one based on specific surface types as defined by the MOD03 geolocation data (i.e. a set of LUTs, with emphasis on distinction between land, coast, deep water and shallow water for reasons explained in the following section) and a version that does not discriminate on surface type (i.e. single LUT). The LUT 'cubes' (with axes formed by the blue, red and NIR band reflectance) are 250 elements on a side. The values at each grid index represent the centres of 0.5%-wide bins of reflectance (i.e. 0.25%, 0.75%, 1.25%, up to 124.75%). Values exceeding 100% are allowed to accommodate certain optically thick side-illuminated clouds (where assumptions in the atmospheric correction software of reflection from a horizontal surface at sea level are violated). The resolution of the LUT defines a low-end uncertainty to the technique and was selected as a trade off between perceivable image quality (variations at the 0.5% level are difficult to detect) and computational efficiency.

To populate the green LUTs ( $\text{LUT}_G$ ), the closest reflectance bin index for each atmospherically corrected band (red, NIR, blue) must first be determined. Two supplemental arrays, each having the same dimensions as the  $\text{LUT}_G$ , are updated with the new information – one increments a counter ( $\text{LUT}_C$ ) for the current (red, NIR, blue) index to keep track of the number of data points tallied for this index, and

the other aggregates ( $LUT_A$ ) the current value of atmospherically corrected green-band reflectance with previously aggregated observations that fell into this index. The updated  $LUT_G$  value at the current index is then given simply by the average value:

$$LUT_G(\text{red, NIR, blue}) = \frac{LUT_A(\text{red, NIR, blue})}{LUT_C(\text{red, NIR, blue})}. \quad (1)$$

The examples shown in this article populate  $LUT_G$  using globally distributed Aqua MODIS data collected during 2009 (Julian days 175–203 and 321–331). These periods were selected arbitrarily and do not necessarily represent an optimal sample for application to the case studies shown in §7, but they do illustrate the general utility of the algorithm to arbitrary scenes even when considering a limited sample. The collection provided an asymptotic population of 15.4% (roughly 2.4 million unique (red, NIR, blue) indices, based on 3.2 billion contributing observations) for the ‘non-discriminating surface’ LUT.

To synthesize the green band information, the algorithm loops over all the pixels of the atmospherically corrected image. At each pixel, the observed (red, NIR, blue) reflectance data are used to locate the closest bounding indices for each dimension of  $LUT_G$ . If a valid  $LUT_G$  value exists at this index, then it is assigned as the synthesized green band value for the current pixel. If a null-value exists in  $LUT_G$  at the current index, then the algorithm attempts an expanded search in the neighbourhood of the index. The search window is incremented iteratively by index values of  $\pm 1$  (or  $\pm 0.5\%$  in reflectance) in each dimension (or else to the bounding dimensions, if reached) centred on the current index, up to a maximum of  $\pm 50$  (or  $\pm 25\%$  in reflectance) until at least two good values are discovered. Even for LUTs developed on the limited data collection mentioned earlier, it was found that only in very rare cases were expanded searches required (e.g. 7000 pixels out of a 44 million, or  $\sim 0.01\%$  for the example shown in figure 1), with the vast majority of these being one-increment expansions. Furthermore, quantitative analyses (presented in §7) indicate that absolute differences with respect to actual green-band reflectance values for these expanded-search-based values are predominantly less than 3%. As a catch-all to the algorithm, any pixel failing the maximum expanded search is assigned a ‘bad’ value of  $-999$ , and these flagged pixels are rendered black in the natural colour image.

Once the green band has been computed per the method outlined earlier, the data are re-mapped to an azimuthal equal-area projection, using the National Snow and Ice Data Center’s (NSIDC’s) MODIS Swath-to-Grid Toolbox (MS2GT; a software package written by Terran Haran and Ken Knowles). Here, a geographic domain is defined based on central latitude, longitude, pixel resolution, and east/west and north/south pixel dimensions of the final image. The red, synthesized green and blue percentage-reflectance bands are then divided by 100 (to provide a decimal form of the reflectance), truncated between  $[0.0223, 1.1]$ , and a  $\log_{10}$  scaling is applied to enhance the relatively dim land/ocean surface portions of the scene at the expense of allocating a lower dynamic range to bright feature (e.g. cloud and snow/ice) details of the scene and mimic the response function of the human eye. The final enhanced MODIS red/green/blue bands, now defined over  $[-1.65, 0.04]$ , are scaled to byte values  $[0, 255]$  and loaded into the respective red, green and blue planes of a TIFF-format image.

Besides its simple construct and ease of implementation, an important strength of the LUT algorithm is that it makes no implicit assumptions on the functional relationship between the spectral bands. The most common relationship found in the data for a given colour index will dominate statistically, and the variation of that relationship across the three-dimensional spectral space is captured. A limitation of the approach is that by its averaging of multiple solutions, certain relationships between green and the (red, NIR, blue) observations that are only valid for particular features may be either compromised or lost altogether (appealing to the aforementioned need for spectral control points, or for the current technique, feature-dependent LUTs). In particular, this problem arises in cases when large values of green reflectance occur for reasons other than the presence of chlorophyll (e.g. shallow or slightly turbid water conditions). Here, values of green are not correlated strongly with the NIR band reflectance, and even the most carefully selected spectral control points may have difficulties in mapping correct values of green from the available (red, NIR, blue) information. Examples of this limitation are provided in §7.

A partial solution to this problem, applicable to the case of shallow water regions and readily produced with the assistance of a static auxiliary database, has been developed here. The auxiliary database, used to define surface classification-dependent LUTs, comes from the MODIS geolocation files (MOD03). These files contain the byte value for each pixel, designating the surface type for that pixel according to the first two columns of table 2. In this data set, shallow ocean corresponds to water, that is either within 5 km of the coastline or less than 50 m deep (based on an ancillary bathymetry database). Likewise, shallow inland water is either within 5 km of the shoreline or less than 50 m deep. Deep inland waters are both 5 km from the coast/shore and  $>50$  m deep. Moderate-depth ocean waters have depths between 50 and 500 m, and deep ocean waters exceed depths of 500 m. The MOD03 classes were consolidated into three main categories (deep water, shallow water and land) for the purposes of capturing the primary colour properties for the current algorithm, and LUTs were constructed for each category. There are no shared-class memberships for a given pixel in the MOD03 database, resulting in spatial discontinuities between the classes. To minimize the possibility of discontinuities in the synthetic imagery at the interfaces between the shallow and deep water categories (e.g. some ‘shallow water’ classification areas in MOD03 hold more similarity to deep water scenes due to the conservative nature of how this class was defined spatially), the synthetic green algorithm first computes a value of green from both the shallow and deep water category LUTs. The blue band reflectance is then used to determine a simple weighted average between the results from each category and assign a final green value for the pixel (higher values of blue reflectance weight the shallow water LUT more heavily, while lower values of blue reflectance weight more heavily the deep water LUT). The approach was found to remove minor but visually discernible colour discontinuities along these category interfaces in the synthetic-green natural colour imagery.

## 7. Results and discussion

This section presents six examples of synthetic-green natural colour imagery rendered under various challenging scenes to demonstrate both the expected performance and limitations of the current algorithm. This assessment is done both qualitatively (via head-to-head comparisons of natural and synthetic imagery) and quantitatively (via direct comparisons between synthetic and actual green band values). While these examples do not offer a comprehensive evaluation of the algorithm, they do provide a

Table 2. MODIS geolocation (MOD03) file information on surface type, used to define and apply surface-type-dependent look-up tables in the current synthetic-green algorithm.

MOD03 byte value	MOD03 surface type	Synthetic-green algorithm category
0	Shallow ocean water	Shallow water
1	Land	Land
2	Ocean coastlines and lake shorelines	Land
3	Shallow inland water	Shallow water
4	Ephemeral water	Land
5	Deep inland water	Deep water
6	Moderate-depth ocean water	Shallow water
7	Deep ocean water	Deep water

Notes: The classifications have been consolidated into three categories. See text for details.

representative cross section of performance based on many other test cases not shown here. With the focus application being to the next-generation GOES imagers, the following cases draw from the geographic coverage provided by the current GOES East (75° W) and West (135° W) satellites. All comparisons are based on MODIS data, which provide a means to self-validate the technique. The main difference between results shown here and capabilities anticipated from the GOES-R ABI are in spatial resolution – current examples are produced at ~250 m resolution while the ABI capability will be ~500 m at nadir (with far superior temporal resolution to MODIS). In a similar fashion to what is done currently with MODIS (which provides only the red and NIR bands at 250 m resolution), the ABI blue band (native 1 km resolution, see table 1) will be increased to 500 m resolution by encoding to it the observed sub-pixel-scale variance observed in the red band (native 500 m resolution).

### 7.1 Biomass smoke over vegetated backgrounds

With the strong reliance of the synthesized green band on values of NIR reflectance, and the relative transparency of smoke in the NIR (small particles exhibit strong blue-light scattering and much weaker NIR scattering), there were some concerns that the algorithm may derive unrealistically large values of synthetic-green reflectance and demonstrate a corresponding green/cyan anomalies in areas of biomass smoke overriding vegetation. To examine this potential issue, several fire cases featuring smoke plumes of varying visible opacity, drifting over various land surface backgrounds including green vegetation, were processed.

Figure 3 compares natural colour and the synthetic-green rendition for a representative case of biomass smoke over vegetation for the midwestern USA on 28 June 2002 (centred on 43.5° N, 89.0° W and 1000 km on a side). The diffuse grey regions covering much of Wisconsin and northern Lake Michigan are smoke plumes originating from wildfires in Saskatchewan, Canada. In general, the algorithm performed well across all portions of the smoke plumes as well as surrounding clear-sky regions over both land and water. The lower panels of figure 3 display the spatial variability of disagreement between the actual green-band reflectance ( $R_G$ , in %) and the synthetic-green reflectance ( $R'_G$ , in %), in terms of both absolute differences:

$$\Delta_{\text{abs}} = R_G - R'_G \quad (2)$$

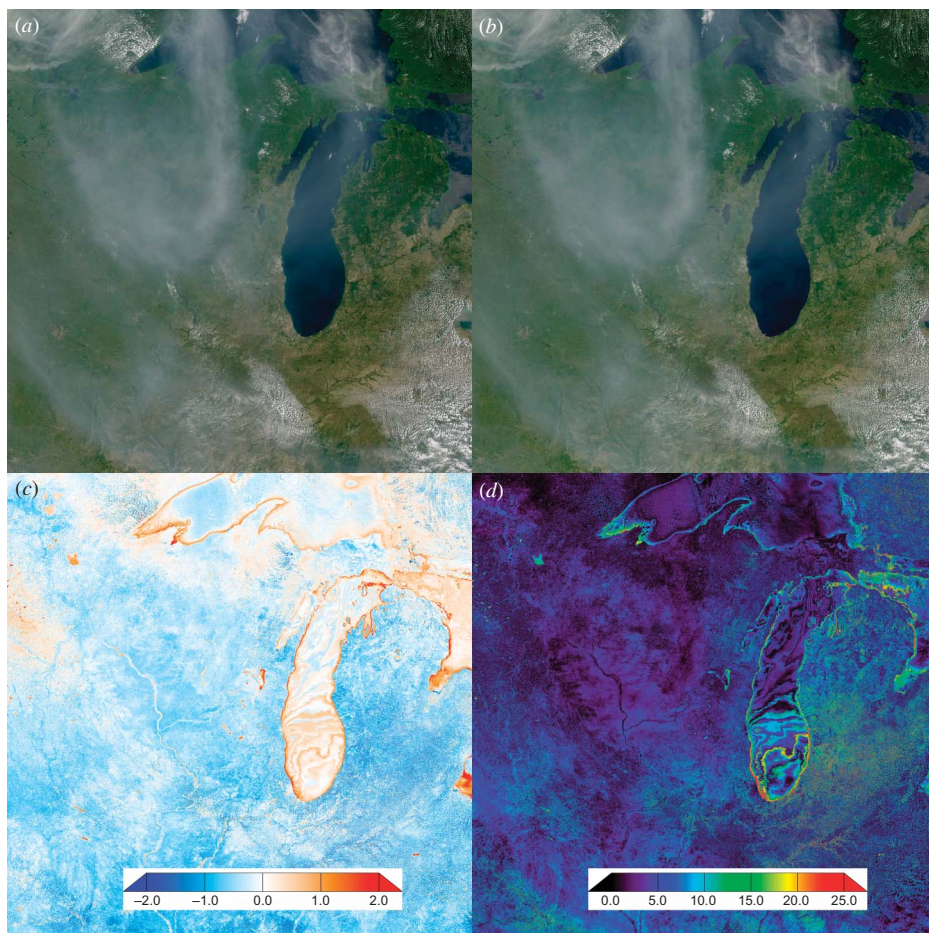


Figure 3. Evaluation of algorithm performance for a smoke-over-vegetation case collected over the Midwestern USA by Terra MODIS on 28 June 2002 at 1640 UTC. Each panel is centred on  $43.5^{\circ}$  N,  $89.0^{\circ}$  W and is 1000 km on a side. (a) shows natural colour, (b) makes use of the synthetic-green band, (c) shows absolute differences (equation (2); units of % reflectance) in terms of actual green minus synthetic green reflectance values and (d) shows relative differences (equation (3); units of %) with respect to the actual green values.

and relative differences:

$$\Delta_{\text{rel}} (\%) = 100 \times \frac{|(R_G - R'_G)|}{R_G}. \quad (3)$$

The relative differences tend to highlight darker portions of the scene where uncertainties in the synthetic-green value present a potentially more dramatic effect in the imagery. In the absolute differences, negative (blue) values correspond to overestimation by the synthetic-green algorithm, while positive (red) values depict areas of underestimation. The relative differences are encoded in a rainbow colour scale ranging from small values in cool (blue) colours and larger values in warm (red) colours. While inspection of figure 3 reveals that most absolute differences are within 1%

reflectance, some areas have relative differences exceeding 20%, particularly for the darker pixels. It is interesting to note the slight high-bias over the land surfaces and low-bias over bodies of water. The behaviour is thought to be related to the abundance of bright green foliage over land surfaces and the scarcity of green over most water bodies, which dominate the average green value for a given blue/red/NIR triplet.

## 7.2 Fall foliage transition

One of the most unique characteristics of natural colour imagery is its ability to capture visually the great variety of vegetation and soil types, and changes in these properties over time. For example, during the fall brilliant colour displays herald the transition to dormancy of mid-latitude deciduous trees as chlorophyll transfer to the leaves shuts down. Chlorophyll is highly reflective in the green part of the spectrum, accounting for the lush green colour of most deciduous trees during the summer months. When chlorophyll concentrations decrease, other chemicals present in the leaves (e.g. carotenoids that reflect yellow/orange, and anthocyanins that reflect purple and red) begin to dominate the reflected sunlight. Although to human vision, this transition results in distinctive colour contrasts depending on the relative concentrations of these residual chemicals, in the NIR these remaining chemicals (carotenoids and anthocyanins) share high reflectance properties similar to chlorophyll (cf. figure 2 of Merzlyak *et al.* 2003). The removal of strong green reflectance, while preserving high values of NIR reflectance, introduces a unique challenge to the current algorithm, which uses the NIR reflectance as the principal source of information for assigning green tonality.

The challenge is illustrated in the series of Terra MODIS images shown in figure 4. The case study covers a region centred over northern Wisconsin (46.0° N, 89.0° W, and 500 km on a side). Figures 4(a), (c) and (e) correspond to late-summer (2 August 2007, 1655 UTC) prior to the onset of fall foliage transition, and figures 4(b), (d) and (f) are from early fall (22 September 2007, 1725 UTC) near the height of fall colours for the region. Figures 4(a) and (b) are the natural colour imagery using the actual green band, figures 4(c) and (d) are the synthetic green version and figures 4(e) and (f) are the reflectance differences between the actual green and synthetic green bands (as in figure 3). The example demonstrates the algorithm's ineffectiveness in capturing the deep orange/red tones of the deciduous forests, with overestimation of green reflectance in some locations by as much as 21% (absolute values of reflectance error) and 200% (relative to the actual green value, and largest for lower values of reflectance).

Recall that the LUT prepared for these demonstrations was based on northern-hemisphere summer and late-fall data, such that little if any information on fall transitional foliage colours was included. However, even after introducing several cases of deciduous forests in fall transition, the appearance of the synthetic imagery (not shown) changed only minimally. The reason for the small change hark back to the fact that the remaining chemicals in the changing leaves preserve a high NIR reflectance, such that non-unique colour indices are populated in the LUTs. In terms of dominating signals in the LUT statistics, the darker earth-tones of the fall foliage coupled with high NIR reflectance may also map to bare-earth scenes, adding further confusion (non-uniqueness) to the database.

Figure 5 shows a version of the 22 September 2007 fall colour imagery (i.e. the right column panels of figure 4) where only the current scene's data are used to populate the

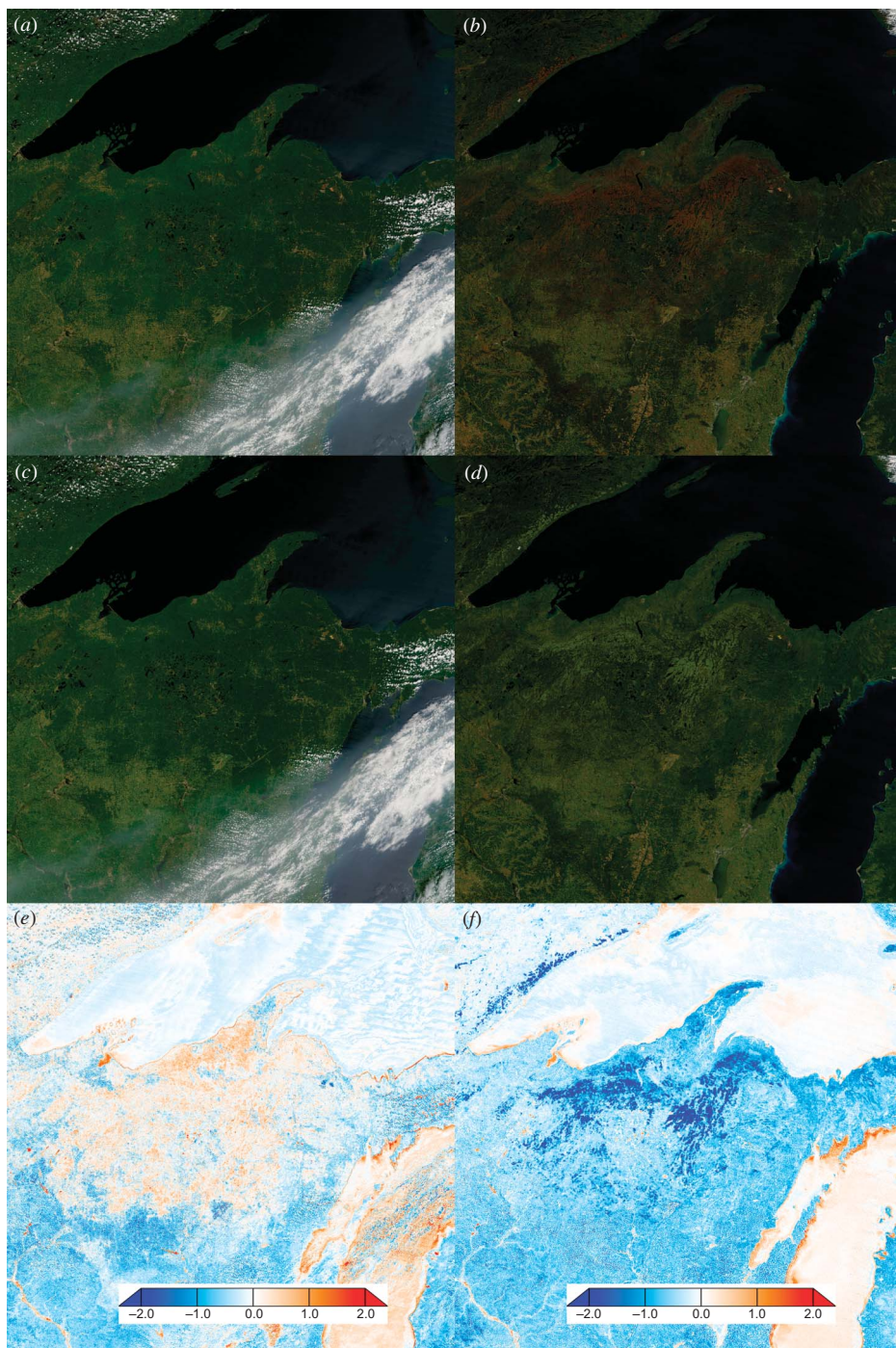


Figure 4. Evaluation of algorithm performance for fall foliage transition over northern Wisconsin. Each panel is centred on  $46.0^{\circ}$  N,  $89.0^{\circ}$  W and is 500 km on a side. (a) and (b) are natural colour validation imagery for 2 August 2007 (Terra MODIS, 1655 UTC) and 22 September 2007 (Terra MODIS, 1725 UTC), respectively. (c) and (d) are the corresponding synthetic images, and (e) and (f) are the corresponding absolute differences (% reflectance) with respect to the actual green values.



Figure 5. Same case study and domain as figure 4 for the 22 September 2007 example, with validation natural colour in (a), a version of synthetic imagery based on a refined LUT (based only on the current scene) in (b) and the absolute differences (% reflectance) with respect to the actual green values (c) showing an overall improvement in comparison to (f) of figure 4.

synthetic-green LUT. While the agreement is much improved, there remain some areas of larger disagreement (10% absolute error). The persistence of these errors is due to the non-unique relationship between the bands and the effects of combining them as an unweighted average. These findings speak of the need for region-specific, time-varying LUTs in order to minimize the effects of non-unique relationships between blue/red/NIR and green-band reflectance. This is an area of future development, and is pointed out here as a limitation of the current algorithm.

### 7.3 Differentiating between dust and smoke

An important analysis capability afforded by natural colour is the discrimination between various surface and atmospheric constituents based on colour differences that are not available from broadband visible measurements. In the fall of 2007, strong, hot and dry Santa Ana winds in Southern California downed power lines over dry vegetation and quickly fanned the flames of wildfires that advanced westward towards heavily populated regions of San Diego and Los Angeles counties. Thick plumes of smoke from the fire lines were accompanied by plumes of dust/debris lifted by the scouring winds over certain barren land surfaces, producing a very complicated scene when viewed from the satellite perspective. Here, the ability to distinguish between various plumes and identify the actual fire threats via colour differences is a potential advantage of natural colour imagery.

Figure 6 examines the ability of the current algorithm to resolve the smoke and dust plumes over portions of Southern and Baja California for the Santa Ana wind event described earlier. The observations were made by Aqua MODIS on 22 October 2007 at 2055 UTC. Each panel is centred on  $33.0^{\circ}$  N,  $117.0^{\circ}$  W and is 800 km on a side. Dust plumes appear tan/brown while wildfire smoke plumes appear light grey. The absolute and relative errors in the algorithm are as in previous examples. While a minor high-green bias is evident (figure 6(c)) in the synthetic-green results for portions of both kinds of plumes, the relative errors (figure 6(d)) are small and colour-based discrimination capabilities are retained in the product imagery.

### 7.4 Ocean colour features

With the deletion of the Hyperspectral Environmental Suite (HES) from the GOES-R instrument manifest, the only remaining capability for parameters related to ocean

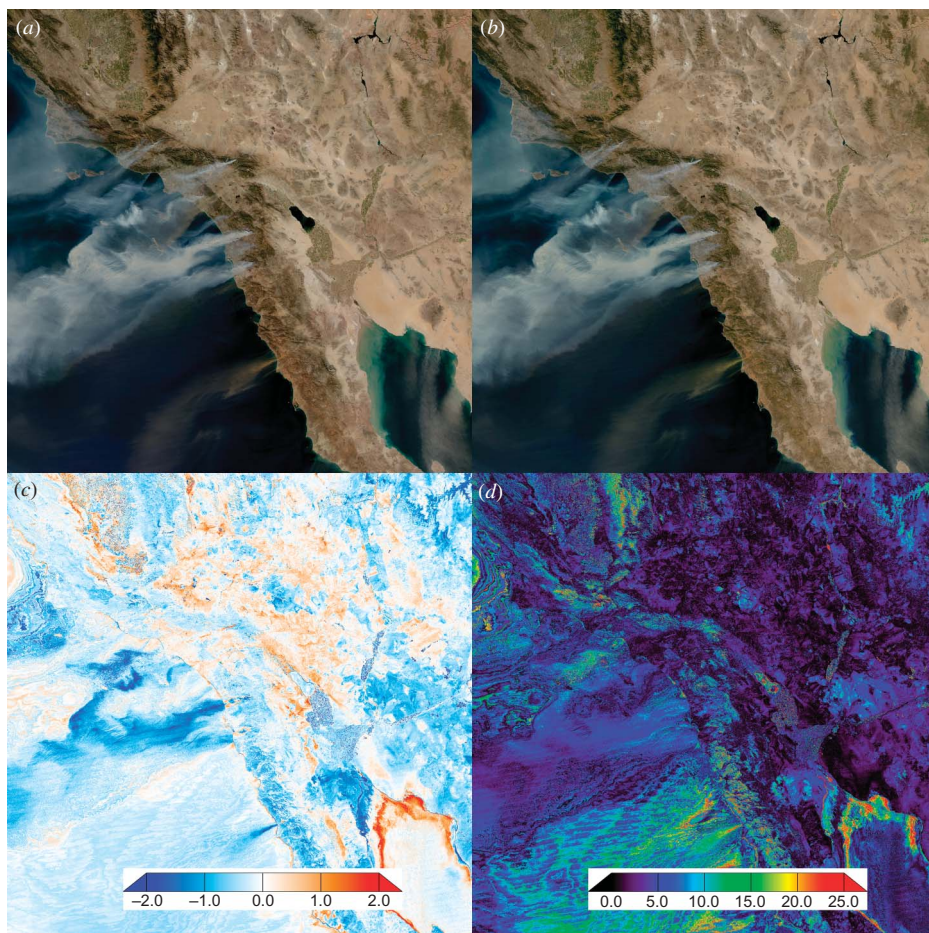


Figure 6. Evaluation of algorithm performance for wildfire smoke and dust plumes during a Santa Ana wind event in Southern California as observed by Aqua MODIS on 22 October 2007 at 2055 UTC. Each panel is centred on  $33.0^{\circ}$  N,  $117.0^{\circ}$  W and is 800 km on a side. Panel descriptions and colour bar units are as in figure 3.

colour research and applications resides with the ABI. Since the ABI channels were not engineered to provide the spectral and radiometric resolution necessary for high-quality quantitative ocean colour applications (e.g. the retrieval of chlorophyll-*a*), the remaining capabilities are limited, but the ABI still offers potentially useful information pertaining to the location, structure and composition of certain biological features. These capabilities are limited by the absence of the green band, as discussed earlier, but recoverable to some extent through the current synthetic-green algorithm.

Shown in figure 7 is an assessment of the synthetic-green algorithm for a phytoplankton bloom that occurred off the coast of Argentina on 16 January 2005, as observed by Aqua MODIS at 1810 UTC. Each panel is centred on  $40.0^{\circ}$  S,  $58.0^{\circ}$  W and is 625 km on a side. Similar to the Bay of Biscay bloom shown in figure 1, the Argentinian bloom appears to contain a variety of species at different stages in development, as inferred by the diversity of colours present. The ability of the algorithm to reconstruct the green component of these colours ranges from good to poor, depending on location in the bloom – better in the brighter portions on the western

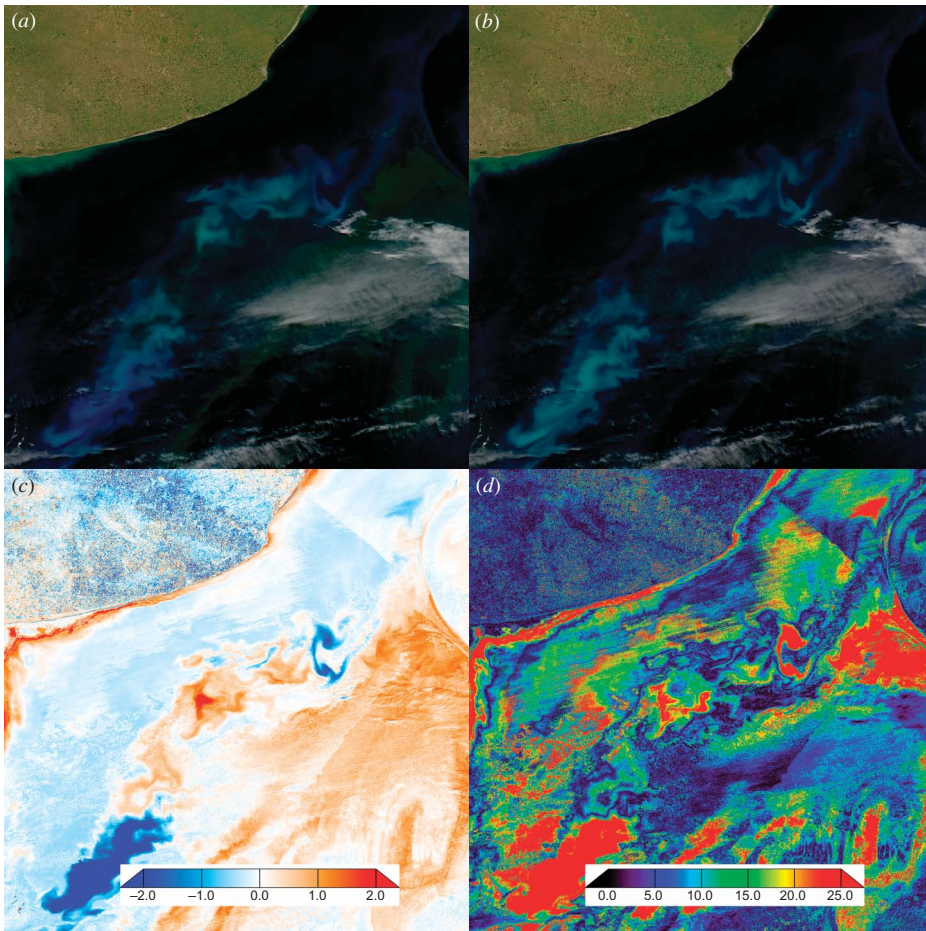


Figure 7. Evaluation of algorithm performance for phytoplankton blooms off the coast of Argentina as observed by Aqua MODIS on 16 January 2005 at 1810 UTC. Each panel is centred on  $40.0^{\circ}$  S,  $58.0^{\circ}$  W and is 625 km on a side. Panel descriptions and colour bar units are as in figure 3.

side and worse in the more pristine green areas on the eastern side. For the latter regions, the weak dependence of the NIR reflectance (water is a strong absorber, even in the presence of the chlorophyll-*a* reflectance) and the absence of strong blue/red signal (accounting for the pristine green appearance) leaves little if any information for the LUT to utilize in providing the correct green value. Similar to the problems of ambiguity in fall foliage, over-water green features are another inherent limitation of the current algorithm that even the most refined (category-dependent) LUTs may not be able to overcome.

### 7.5 Shallow water features

As demonstrated in the preceding examples, the greatest challenges for the current algorithm occur in scenes where values of green are uncorrelated with the available blue/red/NIR information present in the LUTs. Shallow water (e.g. near coastlines,

coral reefs, shoals/sandbars) and some cases of turbid water can take on hues of green that are not due to the presence of chlorophyll-*a*. Here, the NIR reflectance is only weakly correlated with values of green, and the algorithm will fail to reproduce the observed green value.

Figure 8 shows an example of algorithm performance for a particularly challenging scene over the Bahamas as observed by Terra MODIS on 21 January 2003 at 1600 UTC. Each panel is centred on 25.0° N, 79.0° W and is 500 km on a side. The large shoals present in this image produce a rich and variable array of turquoise, aquamarine, and deeper green colours whose green components do not always offer strong correlation with the blue/red/NIR data. Again, the strongest differences (both absolute and relative) tend to occur in shallow water regions of more pristine green tonality, where the blue/red/NIR information offers no clear mapping. Usage of the shallow water specific table helps to overcome these problems to a marginal extent, but as seen

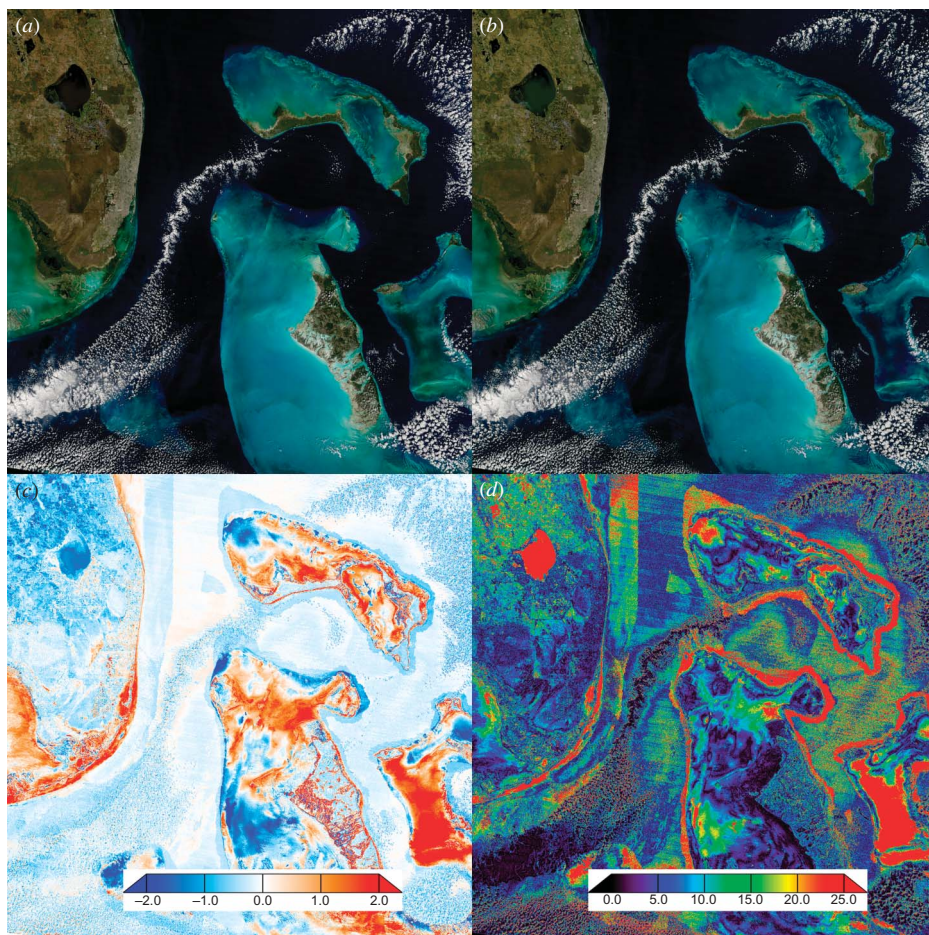


Figure 8. Evaluation of surface-type-dependent algorithm performance for shallow water regions of the Bahamas as observed by Terra MODIS on 21 January 2003 at 1600 UTC. Each panel is centred on 25.0° N, 79.0° W and is 500 km on a side. Panel descriptions and colour bar units are as in figure 3.

in the lower panels of figure 8 the algorithm continues to understate green in the most pristine areas. The synthetic imagery artefacts (e.g. false boundaries) that emerge as a result of where the LUTs succeed/fail in assigning correct values of green may lead to misinterpretation of certain littoral features and should therefore be underscored here as another caveat of this algorithm.

### 7.6 Volcanic ash

The field of regard for the GOES East (75° W) and West (135° W) satellites includes coverage several active volcanoes distributed across the Pacific Rim. Microscopic shards of volcanic glass found in many volcanic ash plumes are known to present a number of significant aviation hazards, including jet engine flame-outs, flight instrument clogging and windshield frosting (e.g. Hobbs *et al.* 1991). International groups such as the Volcanic Ash Advisory Centers, established by the International Civil Aviation Organisation (ICAO) of the United Nations, are charged with monitoring and predicting the dispersion of hazardous volcanic ash plumes, and use satellite imagery to assist in identifying and tracking them.

The physical composition of volcanic ash varies significantly for different volcanoes and even for a given volcano at different stages in its eruption. The most common components are volcanic glass rich in silica content, minerals (such as quartz and feldspar) and other rocks encountered by the rising magma column. In addition to ash, volcanic eruptions emit water vapour, sulphur dioxide, carbon dioxide and other gases in proportions depending on the nature of the volcano. This complicated mixture of ash and gases translates to an equally complex array of potential optical properties across the optical spectrum. Here, natural colour imagery provides some potential insight on ash plume composition through interpretation of colour.

Although outside of the field of view for GOES East coverage, the recent eruptions of the Eyjafjallajökull volcano in Iceland provide a convenient case study for evaluating the performance of the synthetic-green algorithm based on MODIS data. The eruptions commenced on 20 March 2010, after several months of precursor seismic activity, and intermittent activity continued until mid-May 2010 (including a major series of eruptions on 14 April 2010, which resulted in widespread impacts to international commercial aviation). Figure 9 captures an active eruption of Eyjafjallajökull as observed by Terra MODIS on 7 May 2010 at 1235 UTC. Each panel is centred on 63.63° N, 19.62° W and is 500 km on a side. The main plume, tracking towards the southeast, is well-resolved by the synthetic-green algorithm. Also evident is a second plume, originating from near the coast to the east of the volcano and tracking towards the southwest underneath the volcanic plume (as inferred by shadows cast upon it by the latter). It is likely that this second plume is also volcanic ash, deposited by previous eruptions and re-lofted by strong northeasterly surface winds. The natural colour imagery readily distinguishes both plumes from the surrounding cloud structures.

### 7.7 Discussion

The results for all the case studies presented are summarized quantitatively in table 3 in terms of mean, standard deviation, and correlation for both the absolute and relative differences between the actual and synthetic green imagery (as defined in equations (2) and (3)). The overall absolute and relative differences are  $-0.114 \pm 0.567$  (% reflectance) and  $7.768 \pm 7.490$  (%), respectively. Correlation coefficients ( $r$ ) exceed 0.965 for all cases, with a majority exceeding 0.995. The largest relative

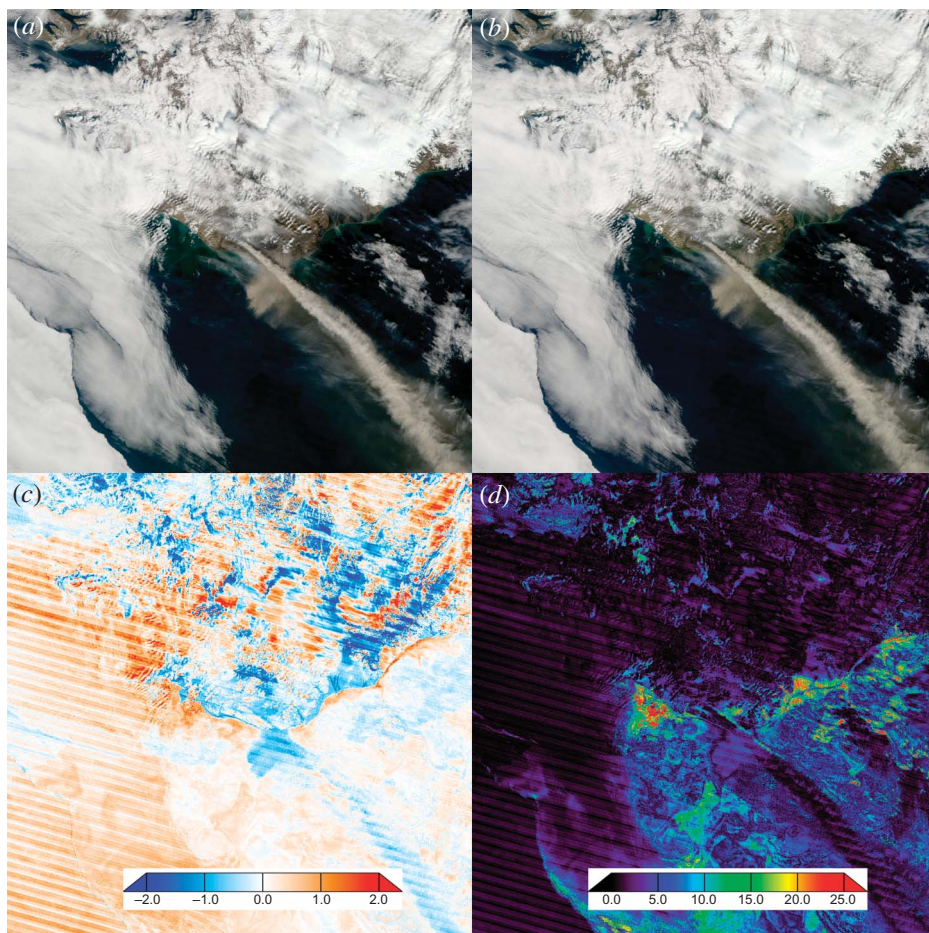


Figure 9. Evaluation of algorithm performance for an eruption of the Eyjafjallajökull volcano in Iceland as observed by Terra MODIS on 7 May 2010 at 1235 UTC. Each panel is centred on the volcano at  $63.63^{\circ}$  N,  $19.62^{\circ}$  W and is 500 km on a side. Panel descriptions and colour bar units are as in figure 3.

errors were found to occur for the fall foliage and the water feature (Bahaman shoals and Argentine phytoplankton bloom) cases, where relatively dark scenes containing ambiguous green contribute significantly to the disagreements. A slight bias towards overestimation of green reflectance is observed in scenes dominated by land surface, while the water-dominant scenes demonstrate a subtle bias towards underestimation of green reflectance (missing some of the green features).

Overall, the results indicate that the synthetic-green algorithm produces good qualitative and quantitative agreement for a majority of scene types. The greatest challenges were found occur for cases where green tonality is uncorrelated or only weakly correlated with the NIR band. While the LUTs may become more generally applicable with additional training data distributed over space and time, they may also average away important local relationships as standard deviations associated with a given B/R/NIR triplet increase (e.g. the fall foliage case study). Generation of LUTs customized to different seasons, specific regions, and scene-type classifications may help

Table 3. Statistical performance (means and standard deviations of the absolute and relative differences as defined in equations (2) and (3), and the correlation coefficient ( $r$ )) of the synthetic-green algorithm for the case studies shown in figures 3–9.

Scene description	Mean $\Delta_{\text{abs}}$	Stdev $\Delta_{\text{abs}}$	Mean $\Delta_{\text{rel}}$ (%)	Stdev $\Delta_{\text{rel}}$ (%)	Correlation ( $r$ )
Midwest smoke over vegetation	-0.2926	0.4754	4.5951	4.3220	0.9974
Midwest summer foliage	-0.1059	0.4562	6.1640	5.5312	0.9990
Midwest autumn foliage	-0.3840	0.5498	12.9166	11.1957	0.9676
Midwest autumn foliage (custom LUT)	-0.1451	0.3274	6.9104	6.5800	0.9859
Southern California smoke and dust	-0.2216	0.4758	4.7926	4.7948	0.9975
Argentina phytoplankton bloom	0.0214	0.6425	11.3428	10.3959	0.9834
Bahamas shoals (combined LUT)	0.0265	0.8323	10.1156	10.5690	0.9990
Bahamas shoals (surface type LUTs)	-0.0471	0.7827	10.2368	10.2866	0.9964
Iceland volcanic ash plume	0.1211	0.5647	2.8414	3.7320	0.9998

Notes: Positive (negative) values mean that actual green values are larger (smaller) than the synthetic version. Results are based on all pixels in each scene.

to minimize these negative effects. The extent to which these artefacts limit the utility of the synthetic natural colour imagery based on the current algorithm will depend on the specific user application.

Since the LUTs used here are based entirely on sun-synchronous MODIS data, it is possible that they will not capture any new colour space arising from different sun/sensor geometry. This sampling limitation is mitigated in part by the 2330 km MODIS swath and 16-day ground track repeat cycle (allowing for various geometries and local viewing times) and the availability of the sensor in both the mid-morning and early-afternoon orbits (Terra and Aqua). In the future, similar LUTs may be created from the JPSS, which will carry the Visible/Infrared Imager/Radiometer Suite (VIIRS) and includes the bands necessary for rendering natural colour imagery. Regardless of the approach, and in light of the physical limitations revealed in the aforementioned examples, it is unlikely that a simulation of the green reflectance can be achieved that results in natural colour imagery devoid of any discernible artefacts under all conditions. The extent to which these artefacts are tolerable by the user community is yet to be determined.

## 8. The challenges of paradigm

The GOES-R ABI sensor was acquired as part of a system procurement process wherein competing vendors submitted bids to design and deliver an instrument meeting the NOAA-specified performance requirements. It is worth noting that a ‘natural colour capability’ was not listed as an explicit requirement of the United States National Weather Service. Although the initial specifications of the ABI were for potentially 18 spectral bands, including a green band to enable natural colour imagery, engineering challenges emerged that forced prioritization of the channel suite. An architecture that accommodated all 18 bands would require additional optical

connections, a higher data rate, and multiple additional circuit cards – additions that would translate to both higher cost and levels of system risk that were viewed as prohibitive. As a result, decision-makers faced a difficult task of prioritizing 16 bands that could be included on available designs of the ABI focal plane array. Through a ranking process that considered the EDR requirements of the GOES programme, the green band received a relatively low priority among the bands, and ultimately was deleted from the notional baseline channel suite.

Factoring into the decision process was the Hyperspectral Environmental Suite (HES) Coastal Waters Imager (CWI), which was still included as part of the GOES-R sensor suite at the time. The CWI would have provided a limited natural colour imaging capability near coastlines, and at superior radiometric and spatial resolutions, albeit not the same spatial/temporal coverage as the ABI. The HES sensor was later deleted from the instrument suite due to concerns over technological risk and affordability, leaving GOES-R with no green band. It is difficult to make a strong case, even in hindsight, for the replacement of any one of the existing 16 ABI channels in favour of a green band. While it could be argued that one of the three ABI bands dedicated to water vapour sounding might have been a candidate, it is perhaps fortuitous that all those bands were retained for the purposes of using the ABI as an atmospheric sounder given the deletion of the HES. One potentially viable option would have been to replace the 1.6  $\mu\text{m}$  band with the green band and use the 2.1  $\mu\text{m}$  band for daytime snow cover detection and cloud phase determination.

The series of events that led to the deletion of a native natural colour capability on GOES-R, despite the demonstrated popularity in the user community and the recognition of imagery as a key capability of the ABI, suggests the existence of a broader, underlying challenge. The development of *ad hoc* work-around algorithms (such as the one presented here) to meet basic performance expectations of the user community speaks to the inherent limitations of what is currently an objective, quantitative-EDR driven instrument design/requirements process. What cannot be escaped, and perhaps is better to simply be accepted at some level beyond the paradigms of science and engineering, is that we derive information content from imagery in ways that we are only able to emulate at first-order by the logic of our most sophisticated algorithms.

The GOES-R ABI design process succeeded in defining imaging performance requirements (spatial, spectral, temporal, and radiometric) for a collection of spectral bands to enable production of numerous EDRs. Here, the ABI channel selection and performance specifications were tied quantitatively to those EDR performance thresholds, and ‘imagery’ was relegated to the visualization of those individual bands (as opposed to imagery resulting from multi-band composites, such as natural colour). In this paradigm, a conundrum exists for natural colour and other red/green/blue composite imagery – despite the general consensus being strong support for such imagery, there is no clear way to quantify that merit in the same way as physical parameters (EDRs). The inability to consider qualitative benefits in an objectively defined process limits in turn the ability to assign priority and ensure these benefits are preserved.

Advancing a qualitatively driven sensor requirement in an inherently quantitatively based field will require a paradigm shift. The current paradigm for defining imagery requirements provides no explicit consideration for multi spectral imagery products such as natural colour. In order to include natural colour as a requirement on future sensors under this paradigm, the concept of imagery quality must be broadened to include an account for the coexistence of multiple bands that are used together to

achieve value-added imagery applications. Otherwise, the term ‘image quality’ is lost in translation between the end users, the procuring agency, and the system designer, and the necessary bands for multi spectral imagery will continue to fall lower in priority to applications having quantifiable performance requirements, regardless of their practical value.

## 9. Conclusion

We have attempted to make a social and scientifically based case for natural colour satellite imagery on the geostationary platform. Although this capability will not be native to the GOES-R ABI, a technique for approximating a green-band reflectance via correlation with spectrally adjacent reflectance measurements in the blue, red, and NIR bands has been developed and demonstrated as a possible mitigation strategy. To develop and demonstrate this technique, MODIS-based atmospherically corrected data were used to construct LUTs that relate the missing green-band reflectance to the other available bands. These LUTs were applied to several independent MODIS case studies as a demonstration of expected performance for such a technique on the GOES-R ABI.

Qualitative results (visual inspection of natural and synthetic imagery) suggest that the synthetic-green technique performs well for many scenes, including challenging situations of highly variable surface/atmosphere composition. Quantitative analysis (relative and absolute differences between the actual and synthetic-green bands) indicates absolute agreement in reflectance (defined over the range (0, 100)) of order 0.1, and relative difference (in units of %) ranging from 5% to 10%, depending on the scene properties. The most significant departures occur for shallow and/or suspended-particle-laden waters (found most commonly in littoral zones, islands, and atolls), and regions of non-green vegetation that retain high near infrared reflectance. The largest relative differences correspond to darker portions of the scene (e.g. over water bodies), do not contribute appreciably to the absolute error and in many cases are very difficult to discern in the RGB imagery products.

The omission from the GOES-R ABI of a native natural colour capability, despite the implicit desire for such imagery among users of geostationary satellite data for decades (as evidenced through its frequent emulation and widespread usage on polar-orbiting satellites), suggests a fundamental flaw in the current process of satellite system design. Specifically, there exists an inherent philosophical challenge to weighing the merits of a qualitative imagery product against quantitative applications. The challenge arises in part from communication failures across paradigms; namely, the desires and expectations related to imagery quality have been distilled and mis-translated to single-band performance requirements rather than the implicit need to consider the complementary nature of the spectral information.

In terms of programme cost savings, enabling natural colour on GOES-R ABI may turn out to be a ‘pay now or pay later’ proposition – initial investment in a green band would have eliminated the research and development investments needed to approximate the desired natural colour performance at some limited level. Necessary improvements to the current synthetic green algorithm include the incorporation of additional shortwave/NIR channels (increasing the LUT dimension), in addition to spatial, seasonal, or class-dependent LUT generation. While we present one method of addressing the synthesis problem here, other approaches that may yield comparable or superior results are also in development. In the end, and after all the investments

have been made to enable a natural colour capability on GOES-R ABI, even the best approach will inevitably fail to reproduce the green band under some sets of circumstances.

The next-generation geostationary satellites to be launched by Europe and Japan both plan to include a green band (along with red and blue) for making natural colour images. The EUMETSAT Meteosat Third Generation (MTG), slated to become operational in 2016, calls for a 0.5  $\mu\text{m}$  band on its Full Disk Imaging (FDI) instrument. The Japan Meteorological Agency (JMA) Himawari-8 and Himawari-9 satellites, scheduled for launches in 2014 and 2016, respectively, will in fact carry 16-band ABI sensors (manufactured by the same commercial vendor) similar in all ways to the capability to those of the GOES-R series, with the exception that the 1.38  $\mu\text{m}$  shortwave water vapour band was deleted in favour of having a green band. Given the demonstrated value of the 1.38  $\mu\text{m}$  band in a number of satellite applications related to the detection and characterization of optically thin cirrus (e.g. Gao and Kaufman 1995), we might anticipate a future article of similar tone to the present one that instead contests the philosophy for preference of a green band. In any case, the decision to include the capability reflects the value of geostationary natural colour to the international user community. The Himawari and MTG data will provide a means to validate the current correlative algorithm for GOES-R ABI directly and in advance of its operational commission (currently slated for 2017).

### Acknowledgements

This work was supported by the Oceanographer of the Navy through the programme office at PEO C4I PMW-120 (PE 0603207N) via Naval Research Laboratory (contract N00173-10-C-2003), and by the NOAA National Environmental Satellite, Data, and Information Service (NESDIS) GOES-R Program Office. We thank Liam Gumley (SSEC/UW-Madison), Jacques Descloitres (NASA/GSFC), and Jeffrey Schmaltz (NASA/GSFC) for software assistance, and Scott Bachmeier (Cooperative Institute for Meteorological Satellite Studies, UW-Madison) for directing us towards useful case studies. The views, opinions, and findings contained in this report are those of the authors and should not be construed as an official NOAA or United States government position, policy, or decision.

### References

- AHN, Y.-H., SHANMUGAM, P., RYU, J.-H. and JEONG, J.-C., 2006, Satellite detection of harmful algal bloom occurrences in Korean waters. *Harmful Algae*, **5**, pp. 213–231.
- BABIN, M., MOREL, A., FOURNIER-SICRE, V., FELL, F. and STRAMSKI, D., 2003, Light scattering properties of marine particles in coastal and open ocean waters as related to the particle mass concentration. *Limnology and Oceanography*, **48**, pp. 843–859.
- BEHRENFELD, M.J., BOSS, E., SIEGEL, D.A. and SHEA, D.M., 2005, Carbon-based ocean productivity and phytoplankton physiology from space. *Global Biogeochemical Cycles*, **19**, GB1006, doi:10.1029/2004GB002299.
- CHEN, C.F. and TSAI, H.T., 1998, A spectral transformation technique for generating SPOT natural colour image. In *Poster Session 3, GIS Development Proceedings, ACRS*, 16–20 November 1998, Manila, Philippines (Tokyo: Asian Association on Remote Sensing (AARS)).
- CHOWDHARY, J., CAIRNS, B., MISCHCHENKO, M.I., HOBBS, P.V., COTA, G.F., REDEMANN, J., RUTLEDGE, K., HOLBEN, B.N. and RUSSELL, E., 2005, Retrieval of aerosol scattering

- and absorption properties from photopolarimetric observations over the ocean during the CLAMS experiment. *Journal of Atmospheric Science*, **62**, pp. 1093–1117.
- CURRAN, P.J. and STEELE, C.M., 2005, MERIS: the rebranding of an ocean sensor. *International Journal of Remote Sensing*, **26**, pp. 1781–1798.
- FALCONE, A.K., AZIMI-SADJADI, M.R. and KANKIEWICZ, J.A., 2007, Dual-satellite cloud product generation using temporally updated canonical coordinate features. *IEEE Transactions on Geoscience & Remote Sensing*, **45**, pp. 1046–1060.
- FROUIN, R. and IACOBELLIS, S.F., 2002, Influence of phytoplankton on the global radiation budget. *Journal of Geophysical Research*, **107**, 4377, doi:10.1029/2001JD000562.
- FU, J., CAULFIELD, H.J., WU, D. and TADESSE, W., 2010, Hyperspectral image analysis using artificial color. *Journal of Applied Remote Sensing*, **4**, 043514, doi:10.1117/1.3374451.
- GAO, B.-C. and KAUFMAN, Y.J., 1995, Selection of the 1.375- $\mu\text{m}$  MODIS channel for remote sensing of cirrus clouds and stratospheric aerosols from space. *Journal of Atmospheric Science*, **52**, pp. 4231–4237.
- GONZALES, C.R., VEEFKIND, J.P. and DE LEEUW, G., 2000, Aerosol optical depth over Europe in August 1997 derived from ATSR-2 data. *Geophysical Research Letters*, **27**, pp. 955–958.
- GOODMAN, S.J., BLAKESLEE, R.J., BOCCIPPIO, D., CHRISTIAN, H., KOSHAK, W. and PETERSEN, W.A., 2006, GOES-R Lightning Mapper (GLM) research and applications risk reduction. Preprints. In *Second Symposium toward a Global Earth Observation System of Systems – Future National Operational Environmental Satellite Systems*, 28 January–2 February 2006, Atlanta, GA (Boston, MA: American Meteorological Society), CD-ROM, p.2.2.
- GORDON, H.R. and CLARK, D.K., 1981, Clear water radiances for atmospheric correction of the coastal zone color scanner imagery. *Applied Optics*, **20**, pp. 4175–4180.
- GURKA, J.J. and DITTBERNER, G.J., 2001, The next-generation GOES instruments: status and potential impact. Preprints. In *Fifth Symposium on Integrated Observing Systems*, 14–18 January 2001, Albuquerque, NM (Boston, MA: American Meteorological Society), CD-ROM, vol. 7.9.
- HO, L.K., JOON, K.Y., VON HOYNINGEN-HUENE, W. and BURROW, J.P., 2006, Influence of land surface effects on MODIS aerosol retrieval using the BAER method over Korea. *International Journal of Remote Sensing*, **27**, pp. 2813–2830.
- HOBBS, P.V., RADKE, L.F., LYONS, J.H., FERREK, R.J., COFFMAN, D.J. and CASADEVALL, T.J., 1991, Airborne measurements of particle and gas emissions from the 1990 volcanic eruptions of Mount Redoubt. *Journal of Geophysical Research*, **96**, pp. 18735–18752.
- KAHRU, M., MTCHELL, B.G., DIAZ, A. and MIURA, M., 2004, MODIS detects a devastating algal bloom in Paracas Bay, Peru. *EOS Transactions of the American Geophysical Union*, **85**, pp. 465–472.
- KING, M.D., KAUFMAN, Y.J., MENZEL, W.P. and TANRÉ, D., 1992, Remote sensing of cloud, aerosol, and water vapor properties from the moderate resolution imaging spectroradiometer (MODIS). *IEEE Transactions on Geoscience and Remote Sensing*, **30**, pp. 2–26.
- MERZLYAK, M.N., SOLOVCHENKO, A.E. and GITELSON, A.A., 2003, Reflectance spectral features and non-destructive estimation of chlorophyll, carotenoid, and anthocyanin content in apple fruit. *Postharvest Biology and Technology*, **27**, pp. 197–211.
- MILLER, S.D., HAWKINS, J.D., KENT, J., TURK, F.J., LEE, T.F., KUCIAUSKAS, A.P., RICHARDSON, K., WADE, R. and HOFFMAN, C., 2006a, *NexSat*: previewing NPOESS/VIIRS imagery capabilities. *Bulletin of the American Meteorological Society*, **87**, pp. 433–446.
- MILLER, S.D., HAWKINS, J.D., LEE, T.F., TURK, F.J., RICHARDSON, K., KUCIAUSKAS, A.P., KENT, J., WADE, R., SKUPNIEWICZ, C.E., CORNELIUS, J., O'NEAL, J., HAGGERTY, P., SPRIETZER, K., LEGG, G., HENEGAR, J. and SEATON, B., 2006b, MODIS provides a

- satellite focus on operation Iraqi freedom. *International Journal of Remote Sensing*, **27**, pp. 1285–1296.
- O'REILLY, J.E., MARITORENA, S., MITCHELL, B.G., SIEGAL, D.A., CARDER, K.L., GRAVER, S.A., KAHRU, M. and McCLAIN, C., 1998, Ocean color chlorophyll algorithms for SeaWiFS. *Journal of Geophysical Research*, **103**, pp. 24937–24953.
- PALTRIDGE, G.W. and PLATT, C.M.R., 1976, *Radiative Processes in Meteorology and Climatology*, p. 318 (New York: Elsevier Scientific Publishing Company).
- PATRA, S.K., SHEKHER, M., SOLANKI, S.S., RAMACHANDRAN, R. and KRISHNAN, R., 2006, A technique for generating natural colour images from false colour composite images. *International Journal of Remote Sensing*, **27**, pp. 2977–2989.
- SABINS, F.F., 1987, *Remote Sensing: Principles and Interpretation*, 2nd ed. (New York: W. H. Freeman and Company).
- SCHMIT, T.J., GUNSHOR, M.M., MENZEL, W.P., GURKA, J.J., LI, J. and BACHMEIER, A.S., 2005, Introducing the next generation advanced baseline imager on GOES-R. *Bulletin of the American Meteorological Society*, **86**, pp. 1079–1096.
- STAMNES, K., LI, W., YAN, B., BARNARD, A., PEGAU, W.S. and STAMNES, J.J., 2003, A new ocean color algorithm: simultaneous retrieval of aerosol optical properties and chlorophyll concentrations. *Applied Optics*, **42**, pp. 939–951.
- SUOMI, V.E. and PARENT, R., 1968, A color view of planet earth. *Bulletin of the American Meteorological Society*, **49**, pp. 74–75.
- TURK, F.J., MILLER, S.D. and CASTELLO, C., 2010, A global cloud layer for virtual globes. *International Journal of Remote Sensing*, **31**, pp. 1898–1914.
- VAN DOLAH, F.M., 2000, Marine algal toxins: origins, health effects, and their increased occurrence. *Environmental Health Perspectives*, **108**, pp. 133–141.
- WANG, L., QU, J.J., XIONG, X., HAO, X., XIE, Y. and CHE, N., 2006, A new method for retrieving band 6 of Aqua MODIS. *IEEE Geoscience and Remote Sensing Letters*, **3**, pp. 267–270.
- WARK, D.Q. and POPHAM, R.W., 1960, TIROS I observations of sea ice in the Gulf of St. Lawrence. *Monthly Weekly Reviews*, **88**, p. 182.
- WARNECKE, G. and SUNDERLIN, W.S., 1968, The first color picture of the Earth taken from the ATS-3 satellite. *Bulletin of the American Meteorological Society*, **49**, pp. 49–83.
- WYSZECKI, G. and STILES, W.S., 1982, *Color Science: Concepts and Methods. Quantitative Data and Formulae*, 2nd ed. (New York: Wiley Series in Pure and Applied Optics).
- YENTSCH, C.S., 1960, The influence of phytoplankton pigments on the colour of sea water. *Deep-Sea Research*, **7**, p. 1.